Synthesis and Characterization of Site-Isolated Hexarhodium Clusters on Titania Powder

Jesse F. Goellner and Bruce C. Gates*

Department of Chemical Engineering and Materials Science, University of California, Davis, California 95616

Received: October 31, 2000; In Final Form: February 12, 2001

$[Rh_6(CO)_{16}]$ was prepared on the surface of TiO_2 (calcined at 200 or 400 °C) by deposition from *n*-hexane solution and by a surface-mediated synthesis from TiO_2-supported $[Rh(CO)_2(acac)]$ in the presence of CO at 1 atm and 100 °C. The cluster preparation and subsequent decarbonylation by treatment in He or H_2 were characterized by infrared and extended X-ray absorption fine structure (EXAFS) spectroscopies. Deposition from solution gave aggregated $[Rh_6(CO)_{16}]$ on TiO_2; removal of the carbonyl ligands led to destruction of the Rh_6 frame and sintering to give rhodium aggregates. In contrast, the reductive carbonylation of TiO_2-supported $[Rh(CO)_2(acac)]$ gave site-isolated TiO_2-supported $[Rh_6(CO)_{16}]$ in high yield, paralleling the chemistry of rhodium carbonyls in neutral solutions and on neutral surfaces. Removal of the carbonyl ligands from the site-isolated clusters by treatment in H_2 at 300 °C led to rhodium aggregates, but decarbonylation in He at 300 °C gave site-isolated Rh_6 clusters on the TiO_2. The first-shell Rh−Rh coordination number of these clusters was 4.4 ± 0.4 with a bond distance of 2.64 ± 0.03 Å. Thus, the clusters formed by decarbonylation of site-isolated TiO_2-supported $[Rh_6(CO)_{16}]$ are represented as octahedral Rh_6 (which has a Rh−Rh first-shell coordination number of 4). EXAFS spectroscopy indicates that the decarbonylated Rh_6 clusters on TiO_2 calcined at 200 °C have a small amount of carbon bonded to them, but no such ligands were indicated in the spectra of the Rh_6 clusters on TiO_2 calcined at 400 °C.

Introduction

Site-isolated metal clusters are important catalysts both in nature and industry. For example, Cu_4 bound to histidine ligands in nitrous oxide reductase catalyzes denitrification.[1] Platinum clusters with nuclearities in the range of about of 5−12 atoms, supported in LTL zeolite, catalyze naphtha dehydrocyclization in the manufacture of benzene.[2] The goal of understanding the influence of the ligands and supports for such clusters on their catalytic activity motivates the preparation of uniform supported metal clusters that can be characterized precisely. A successful synthetic method entails the preparation of precursor supported molecular metal carbonyl clusters followed by removal of the carbonyl ligands without significant perturbation of the metal frame.[3]

One of the few techniques that is well suited to the characterization of supported metal clusters is extended X-ray absorption fine structure (EXAFS) spectroscopy, which provides accurate structure data representing the metal frame and information about the metal−support interface.[4] Because the surfaces of supports are usually nonuniform, data characterizations of the metal−support interface are typically not very informative; thus, there is a motivation for using nearly planar supports, such as single crystals, to allow characterization by scanning tunneling microscopy (STM). Because TiO_2 has a small band gap relative to that of other common metal oxide catalyst supports, images of metal particles supported on TiO_2 single crystals[5] or thin films grown on a conducting substrate (e.g., a Mo single crystal[6]) have been found to be of better quality than images of metal particles on other metal oxides.

Consequently, our objective was to investigate nearly uniform metal clusters on TiO_2 powders to lay the foundation for complementary work with such clusters on nearly planar TiO_2 supports. The precursor was chosen to be $[Rh_6(CO)_{16}]$ because methods for preparing this precursor on other supports (e.g., γ-Al_2O_3[7] and zeolites NaY[8] and NaX[9]) have been developed. We report the synthesis and characterization, by infrared and EXAFS spectroscopies, of TiO_2-supported $[Rh_6(CO)_{16}]$ formed by two different methods: (1) deposition of $[Rh_6(CO)_{16}]$ and (2) surface-mediated synthesis involving reductive carbonylation of TiO_2-supported $[Rh(CO)_2(acac)]$. We also report the stability of the Rh_6 frame during treatment to remove the carbonyl ligands, in some cases forming nearly uniform site-isolated TiO_2-supported Rh_6.

Experimental Section

Materials and Sample Preparation. Sample syntheses and transfers were performed in the absence of moisture and air with a Braun MB-150M drybox (purged with N_2 recirculating through traps containing particles of Cu and of zeolite 4A for removal of O_2 and moisture) and a double manifold Schlenk vacuum line. N_2, H_2, and He (each 99.999%, Matheson) flowed through similar traps to remove traces of O_2 and water, respectively. CO (CP grade, Matheson) was further purified by passage through a trap containing particles of zeolite 4A and activated γ-Al_2O_3 to remove traces of water and metal carbonyls from the high-pressure gas cylinder, respectively. Tetrahydrofuran (THF) and *n*-hexane solvents were dried over sodium benzophenone ketyl and deoxygenated with flowing N_2 prior to use. Bis(triphenylphosphoranylidene)ammonium chloride, [PPN]Cl (Aldrich), dicarbonylacetylacetonato rhodium(I), $[Rh(CO)_2(acac)]$, (Strem, 99%), and $[Rh_6(CO)_{16}]$ (Strem, 98%) were used as received.

Deionized water was added to the TiO_2 support (Degussa, P25 TiO_2) to form a paste, which was dried in air at 120 °C overnight. The dried TiO_2 was ground and calcined as O_2 flowed through a bed of the material while the temperature was ramped

* To whom correspondence should be addressed.

10.1021/jp0040291 CCC: $20.00
Published on Web 03/31/2001

TABLE 1: Crystallographic Data Characterizing the Reference Compounds and Fourier Transform Ranges Used in the EXAFS Analysis

		crystallographic data			Fourier transform		
ref compd	shell	*N*	*R* (Å)	ref	Δk (Å^{-1})	Δr (Å)	n[a]
Rh foil	Rh−Rh 1st shell	12	2.687	17	2.86−19.60	1.60−3.12	3
Rh crystal[b]	Rh−Rh 2nd shell	6	3.796	17	1.00−20.00	0.00−8.00	0
Rh crystal[b]	Rh−Rh 3rd shell	24	4.649	17	1.00−20.00	0.00−8.00	0
Rh crystal[b]	Rh−Rh 4th shell	12	5.368	17	1.00−20.00	0.00−8.00	0
Rh_2O_3	Rh−O	6	2.050	22	2.67−15.69	0.00−2.10	2
$[Ru_3(CO)_{12}]$	Ru−C[c]	4	1.910	23	3.71−14.80	0.95−1.87	1
	Ru−O*[d]	4	3.050	23	3.75−14.80	1.90−3.11	2
RhTi alloy[b]	Rh−TiO_2	8	3.392	18	0.00−20.00	0.00−8.00	0

[a] A k^n-weighting was used when taking the Fourier transform of the data for purposes of extracting the reference phase and amplitude functions of the absorber−backscatterer pair. [b] This reference file was calculated by using the FEFF 7.0 software.[16] [c] Used as the reference phase shift and backscattering amplitude for the Rh−C shells. [d] Used as the reference phase shift and backscattering amplitude for the Rh−O* shells.

to the value referred to as the calcination temperature (200 or 400 °C) and held for 2 h. The O_2 treatment was followed immediately by evacuation of the sample for 14 h at the calcination temperature. The TiO_2 was then cooled to room temperature under vacuum, isolated, and stored in a N_2-filled glovebox until use. The resultant samples that had been calcined at 200 and at 400 °C are referred to as $TiO_{2,200}$ and $TiO_{2,400}$, respectively.

In the drybox, a precursor, $[Rh_6(CO)_{16}]$ or $[Rh(CO)_2(acac)]$, was combined with the calcined TiO_2 powder and placed in a Schlenk flask, with the solid mixture containing 1 wt % Rh. Dried and deoxygenated *n*-hexane was then introduced by cannula into each sample in a Schlenk flask, giving a slurry that was stirred for 1 day. The solvent was removed by evacuation (pressure $<10^{-3}$ Torr) for 1 day, and the resultant samples were stored in the drybox. Samples made from $[Rh(CO)_2(acac)]$ were further treated in a once-through flow reactor with CO at 1 atm and 100 °C for 1 day to form TiO_2-supported rhodium cluster carbonyls by surface-mediated synthesis.[10] These were decarbonylated in a once-through flow system, either a glass reactor or an EXAFS cell,[11] by heating in He or H_2 at 1 atm.

Characterization by Infrared Spectroscopy. A Bruker IFS 66v spectrometer with a spectral resolution of 4 cm^{-1} was used to collect infrared spectra of the sample powders. To prepare an optically thin sample allowing detection of minor peaks, a small amount of powder was pressed between two KBr windows of an environmentally controlled infrared cell. Each reported spectrum is the average of 64 scans.

Extraction of Rhodium Carbonyls from TiO_2. Surface-bound rhodium carbonyls were extracted from the TiO_2 surface by contacting the solid in a Schlenk flask with a deoxygenated solution of THF or [PPN]Cl in THF. The mixtures were stirred for approximately 1/2 h and allowed to settle for at least 8 h. The supernatant solution was transferred by syringe into a solution infrared cell, and the cell was sealed and the sample quickly scanned. The spectrum of THF was subtracted from each spectrum, which is the average of 64 scans.

Characterization by EXAFS Spectroscopy. EXAFS spectra were collected at beam line 2−3 of the Stanford Synchrotron Radiation Laboratory (SSRL), Stanford, California, and at beamline X-11A at the National Synchrotron Light Source (NSLS), Upton, NY. The ring current at SSRL was 50−100 mA, and the storage ring operated with an electron energy of 3 GeV. The ring current as NSLS was 110−250 mA, and the storage ring operated with an electron energy of 2.5 GeV.

In a N_2-filled drybox at the synchrotron, each powder sample was pressed into a self-supporting wafer. The mass was chosen to give an X-ray absorbance of approximately 2.5 at the Rh K edge. The wafer was loaded into an EXAFS cell,[11] sealed under a positive N_2 pressure, and removed from the drybox. The cell was then evacuated (10^{-5} Torr), and the sample was aligned in the X-ray beam and cooled to nearly liquid nitrogen temperature. EXAFS spectra were then collected in transmission mode. The double-crystal monochromator (Si(220) at SSRL and Si(111) at NSLS) was detuned by 20% at the Rh K edge to suppress higher harmonics in the X-ray beam.

After EXAFS spectra had been recorded, the samples were removed from the beamline and then further treated in the EXAFS cell for 2 h with flowing He or H_2 at a temperature between 100 and 400 °C. The cell was then cooled to room temperature, reevacuated to 10^{-5} Torr, and cooled to nearly liquid nitrogen temperature. The sample was then scanned as described above.

Analysis of EXAFS Data

Fitting of the EXAFS data was carried out with a difference file technique,[8,12,13] using the software XDAP.[14] Iterative fitting was carried out until excellent agreement was attained between the calculated k^0-, k^1-, k^2-, and k^3-weighted data (k is the wave vector) and the postulated model.[8,12,13]

Experimentally determined reference files prepared from EXAFS data representing materials of known structure were used in the analysis. EXAFS data characterizing rhodium foil and Rh_2O_3 powder were used for the phase shifts and backscattering amplitudes of the first-shell Rh−Rh and Rh−$O_{support}$ interactions. $[Ru_3(CO)_{12}]$ (which has only terminal CO ligands) mixed with X-ray-transparent BN was used to obtain the phase shifts and backscattering amplitudes for analysis of the Rh−C and Rh−O* interactions (O* is carbonyl oxygen). (The transferability of the phase shifts and backscattering amplitudes for neighboring atoms in the periodic table has been justified experimentally.[15]) It was necessary to use a reference that exhibited multiple scattering, such as $[Ru_3(CO)_{12}]$, because the near linearity of the Rh−C−O moieties of terminally bound CO in the samples makes the influence of multiple scattering significant. The second and higher Rh−Rh shell and the Rh−Ti reference files were calculated by using the code FEFF 7.0[16] and experimental structural parameters representing a rhodium crystal[17] and Rh−Ti alloy,[18] respectively. Details of the preparation of the reference files are presented elsewhere.[19,20,21] Table 1 is a summary of the parameters[17,18,22,23] used to construct the reference files from the EXAFS data.

The number of parameters used in fitting the data to each model and the number of parameters justified statistically according to the Nyquist theorem[24] are given in Supporting Information Table 1. The fitting ranges in both momentum space

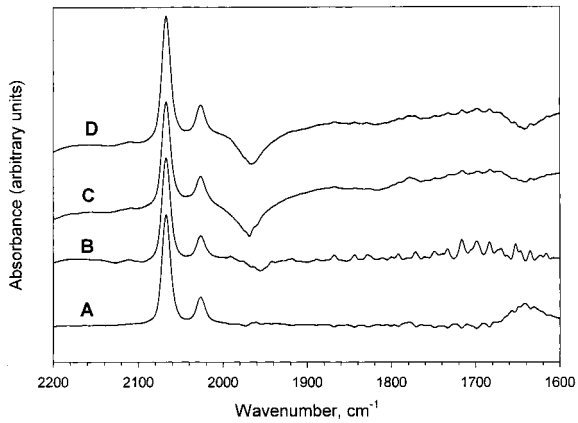

Figure 1. Infrared spectra in the carbonyl stretching region of the extract solution formed by bringing TiO_2-supported rhodium carbonyls in contact with THF. (A) $[Rh_6(CO)_{16}]$ in THF solvent; (B) species formed by deposition of $[Rh_6(CO)_{16}]$ on TiO_2 calcined at 200 °C; (C) species formed by chemisorption of $[Rh(CO)_2(acac)]$ on TiO_2 calcined at 200 °C following treatment in CO at 100 °C for 24 h; (D) species formed by chemisorption of $[Rh(CO)_2(acac)]$ on TiO_2 calcined at 400 °C following treatment in CO at 100 °C for 24 h.

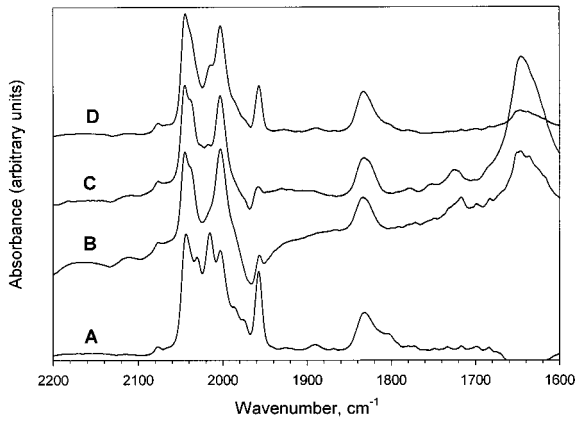

Figure 2. Infrared spectra in the carbonyl stretching region of the extract solution formed by bringing TiO_2-supported rhodium carbonyls in contact with [PPN]Cl in THF. (A) $[Rh_6(CO)_{16}]$ in [PPN]Cl-THF solution; (B) species formed by deposition of $[Rh_6(CO)_{16}]$ on TiO_2 calcined at 200 °C; (C) species formed by chemisorption of $[Rh(CO)_2(acac)]$ on TiO_2 calcined at 200 °C following treatment in CO at 100 °C for 24 h; (D) species formed by chemisorption of $[Rh(CO)_2(acac)]$ on TiO_2 calcined at 400 °C following treatment in CO at 100 °C for 24 h; (E) species formed by deposition of $[Rh_6(CO)_{16}]$ on TiO_2 calcined at 400 °C.

and real space (Supporting Information Table 1) were determined by the data quality. The value of fit diagnostic parameters, ϵ_ν^2 (goodness of fit),[24] and the variances between the data and model prediction for the EXAFS function, χ, and the Fourier transform of χ (for k^0-, k^1-, k^2-, and k^3-weighting of the data) are also summarized in Supporting Information Table 1.

Results

TiO_2-Supported $[Rh_6(CO)_{16}]$ Aggregates formed by Deposition of $[Rh_6(CO)_{16}]$ from Solution. Infrared spectroscopy was used to characterize the deposits of $[Rh_6(CO)_{16}]$ on TiO_2. The ν_{CO} infrared spectrum of the species extracted from the surface of $TiO_{2,200}$ into THF solution (2076 s, 2044 m, 2020 w, 1809 m cm^{-1}) nearly matches that of $[Rh_6(CO)_{16}]$ in THF solution (2075 vs, 2043 w, 1809 m cm^{-1}, Figure 1); evidently $[Rh_6(CO)_{16}]$ had been deposited intact on the support. In contrast, no metal carbonyls were extracted from $TiO_{2,400}$ into THF alone,

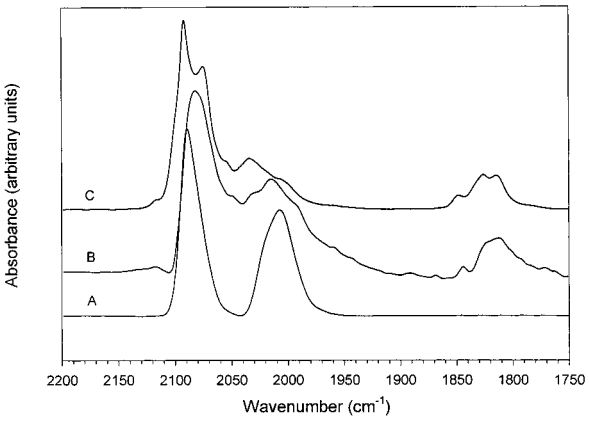

Figure 3. Infrared spectra in the carbonyl stretching region of rhodium carbonyls supported on TiO_2 calcined at 200 °C. (A) Species formed by chemisorption of $[Rh(CO)_2(acac)]$; (B) species formed by chemisorption of $[Rh(CO)_2(acac)]$ followed by treatment in CO at 100 °C for 24 h; (C) species formed by deposition of $[Rh_6(CO)_{16}]$.

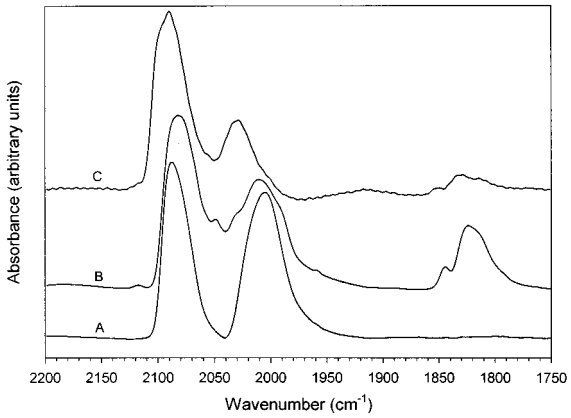

Figure 4. Infrared spectra in the carbonyl stretching region of rhodium carbonyls supported on TiO_2 calcined at 400 °C. (A) Species formed by chemisorption of $[Rh(CO)_2(acac)]$; (B) species formed by chemisorption of $[Rh(CO)_2(acac)]$ followed by treatment in CO at 100 °C for 24 h; (C) species formed by deposition of $[Rh_6(CO)_{16}]$.

which implies that the metal carbonyls were held more strongly to the surface of $TiO_{2,400}$ than to that of $TiO_{2,200}$.

When the surface species were extracted into THF solutions of [PPN]Cl, the infrared spectrum of each sample nearly matched that of $[Rh_6(CO)_{16}]$ dissolved in [PPN]Cl in THF (2056 vs, 2019 m, 1976 w, 1830 w cm^{-1}, Figure 2). The ν_{CO} spectrum of the extract from $TiO_{2,200}$ was 2055 vs, 2019 w, 1976 s, 1830 vw, 1792 m cm^{-1} and that of the extract from $TiO_{2,400}$ was 2054 s, 2008 m-sh, 1975 vs, 1792 m cm^{-1}. As only species consistent with $[Rh_6(CO)_{16}]$ on the TiO_2 surface were extracted with either THF or a solution of [PPN]Cl in THF, we conclude that there had been no significant change in the structure of $[Rh_6(CO)_{16}]$ upon deposition.

The ν_{CO} region of the infrared spectrum[25] of the solid sample made from $[Rh_6(CO)_{16}]$ and $TiO_{2,200}$ (2092 s, 2075 s-sh, 2034 m, 2020 m-sh, 1848 w-sh, 1826 m, 1814 m-sh cm^{-1}, Figure 3) and that of the sample made from $[Rh_6(CO)_{16}]$ and $TiO_{2,400}$ (2092 vs, 2029 m, 1854 vs, 1835 w cm^{-1} , Figure 4) are similar to the spectrum of $[Rh_6(CO)_{16}]$ in KBr (2073, 2026, 1800 cm^{-1})[26] and in THF solution (Table 2, Figure 1). The ν_{CO} bands of the supported $[Rh_6(CO)_{16}]$ are shifted and broadened (and to some extent split) relative to those of $[Rh_6(CO)_{16}]$ in solution, as expected for metal carbonyls on a polarizing nonuniform support such as TiO_2.

TABLE 2: Infrared Bands in the CO Stretching Region Characterizing Supported and Unsupported Rhodium Carbonyls

support (calcination temperature, °C)	precursor	CO treatment conditions	ν_{CO} (cm^{-1}) spectra of the solid	Solution Spectra of Dissolved or Extracted Species: THF	Solution Spectra of Dissolved or Extracted Species: [PPN]Cl + THF	ref
TiO_2 (200)	$[Rh(CO)_2(acac)]$	no treatment	2083 s, 2004 vs			this work
		100 °C, 1 day	2086 vs, 2032 m-sh, 2020 s, 1894 w, 1847 w-sh, 1828 m	2075 vs, 2043 w-sh, 1995 m, 1808 m	2055 s, 2019 w, 1974 vs, 1837 vw,	this work
	$[Rh_6(CO)_{16}]$	no treatment	2092 s, 2075 s-sh, 2034 m, 2020 m-sh, 1848 w-sh	2076 s, 2044 m, 2020 w, 1809 m	2055 vs, 2019 w, 1976 s, 1830 w, 1792 m	this work
TiO_2 (400)	$[Rh(CO)_2(acac)]$	no treatment	2091 vs, 2017 s			this work
		100 °C, 1 day	2118 vw, 2078 vs, 2050 m-sh, 2013 s, 1990 sh, 1846 w-sh, 1827 m, 1702 m	2076 vs, 2043 w, 1809 m	2055 vs, 2019 w, 1975 s, 1832 vw	this work
	$[Rh_6(CO)_{16}]$	no treatment	2092 vs, 2029 m, 1854 vs, 1835 w		2054 s, 2008 m-sh, 1975 vs, 1792 m	this work
γ-Al_2O_3 (400)	$[Rh(CO)_2(acac)]$	no treatment	2092 s, 2014 vs			31
		100 °C, 1 day	2093 s, 2058 m-sh, 2017 vs, 1827 w		2054 s, 1974 vs, 1828 vw, 1780 vw	31
	$[Rh_6(CO)_{16}]$	no treatment	2093 s-sh, 2069 vs, 2027 s, 1837 m-br			7
Zeolite NaY (200 or 300)	$[Rh(CO)_2(acac)]$	no treatment	2082 s, 2014 vs			8
		125 °C, 12 h	2130 w, 2097 s, 2068 sh, 2020 w, 1760 s			8
Zeolite NaX (300)	$[Rh(CO)_2(acac)]$	no treatment	2087 s, 2006 vs			9
		125 °C, 12 h	2100 w, 2050 sh, 2015 s, 1995 sh, 1738 sh			9
Al_2O_3	Rh aggregates	no treatment	terminal: 2060−2040 (1 peak) bridging: 1850			54
Nujol	$[Rh_6(CO)_{16}]$		2105 w, 2070 s, 2047 w, 2040 w, 2022 mw, 2020 mw 1833 w, 1793 s	2075 vs, 2043 w, 1809 m	2056 vs, 2044 sh, 2019 m, 1976 w, 1830 w, 1795 m	55, this work
KBr	$[Rh_6(CO)_{16}]$		2073, 2026, 1800			26

TABLE 3: EXAFS Parameters Characterizing Rhodium Clusters Formed by Deposition of $[Rh_6(CO)_{16}]$ on TiO_2 and Subsequent Thermal Treatment.

TiO_2 calcined at 200 °C: backscatterer (shell)	N	R (Å)	$10^3 \times \Delta\sigma^2$ (Å^2)	ΔE_0 (eV)	treatment	TiO_2 calcined at 400 °C: backscatterer (shell)	N	R (Å)	$10^3 \times \Delta\sigma^2$ (Å^2)	ΔE_0 (eV)
Rh					none	Rh				
(1st)	3.8	2.75	1.78	4.11		(1st)	3.9	2.74	2.83	4.14
(2nd)	0.7	3.91	7.34	0.76		CO				
(3rd)	1.5	4.67	9.95	0.6		terminal				
CO						C	2.3	1.85	1.09	6.10
terminal						O*	2.5	2.99	−1.10	−0.32
C	2.0	1.87	6.33	0.61		bridging				
O*	2.3	2.99	−1.48	0.98		C	3.0	2.11	1.68	2.38
bridging						support				
C	2.4	2.19	1.66	8.83		O				
support					300 °C in He	Rh				
O	0.9	2.12	−2.38	−18.67		(1st)	4.4	2.69	−0.97	−4.63
Rh						(2nd)	1.2	3.80	3.19	−0.75
(1st)	9.3	2.67	1.17	0.40		(3rd)	2.6	4.66	2.62	2.08
(2nd)	1.3	3.80	1.11	−2.16		support				
(3rd)	3.6	4.65	2.14	0.16		O	1.6	2.07	2.46	−0.54
(4th)	2.1	5.28	0.12	−3.74		Ti	2.6	2.98	3.10	1.43
support					300 °C in H_2	Rh				
O						(1st)	5.2	2.64	4.70	1.90
Ti	1.1	3.63	2.85	−17.51		(2nd)				
Rh						(3rd)	1.0	4.65	1.65	−0.94
(1st)	7.5	2.67	2.09	1.64		support				
(2nd)	0.4	3.84	4.62	12.34		O	1.6	2.05	0.49	−6.83
(3rd)	3.3	4.66	4.95	0.42		Ti	0.2	3.99	−0.70	0.10
(4th)	2.3	5.36	3.26	−7.79						
support										
O										
Ti	1.3	3.99	0.00	−0.77						

The EXAFS data (Table 3) support the conclusion that there was no fragmentation of the octahedral Rh_6 frame upon deposition of $[Rh_6(CO)_{16}]$ on TiO_2, within the typical EXAFS error bounds (N, ± 10%; R, ± 0.02 Å; $\Delta\sigma^2$, ± 20%; ΔE_0, ± 20%, where N is the coordination number of the contribution; R the distance from the absorber (Rh) atom to the backscatterer atom; $\Delta\sigma^2$ the Debye−Waller factor relative to the reference material; and ΔE_0 the inner potential correction relative to the reference material.[27] The Rh−Rh first-shell contributions (N = 3.8, R = 2.75 Å and N = 3.9, R = 2.74 Å characterizing the samples supported on $TiO_{2,200}$ and $TiO_{2,400}$, respectively) are consistent with Rh_6 octahedra (N = 4). No higher Rh−Rh shells

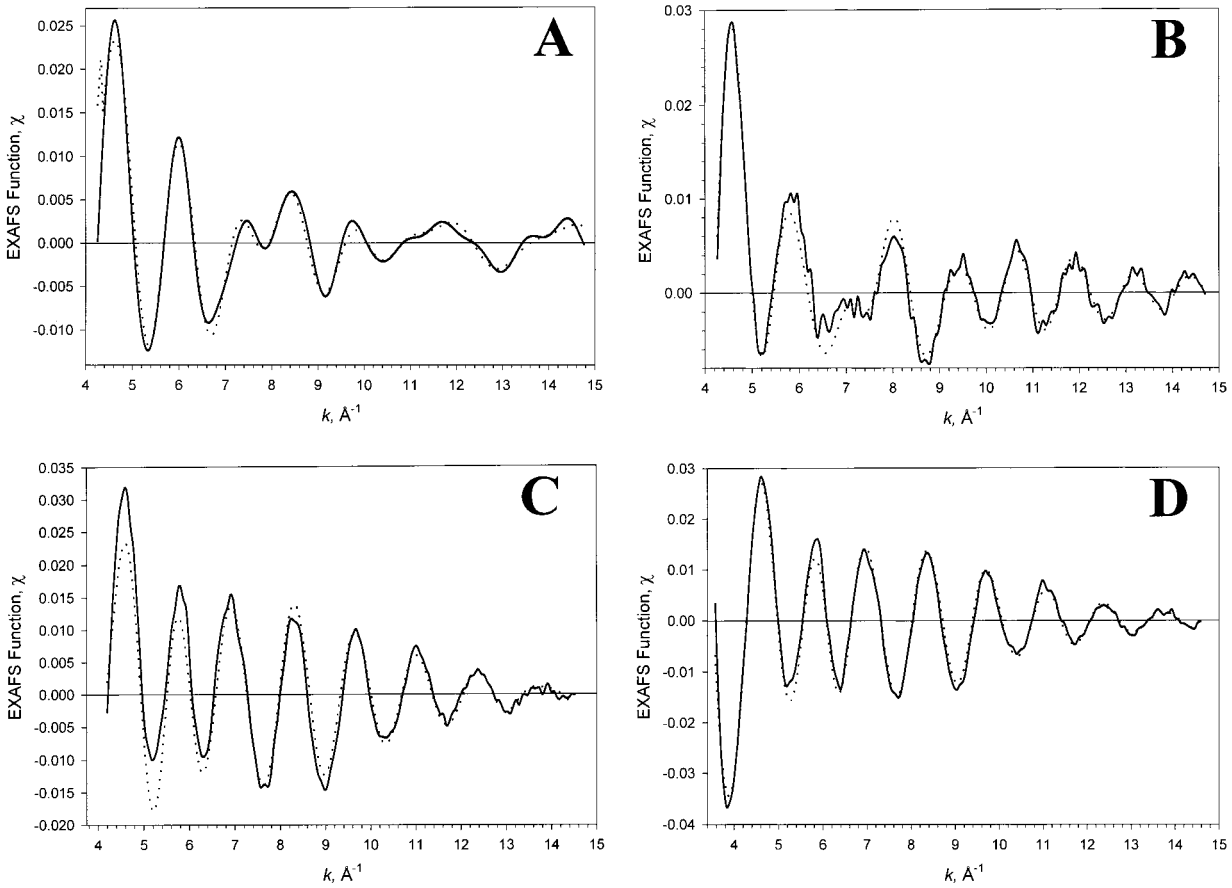

Figure 5. Results of EXAFS data analysis for TiO_2-supported rhodium carbonyls and surface species formed by decarbonylation of rhodium carbonyls: EXAFS function, χ (solid lines) and calculated contributions (dotted lines) according to the reported structural parameters. (A) Species formed by chemisorption of $[Rh(CO)_2(acac)]$ on TiO_2 calcined at 400 °C; (B) species formed by chemisorption of $[Rh(CO)_2(acac)]$ on TiO_2 calcined at 400 °C and subsequent treatment in CO at 100 °C for 24 h; (C) species formed by chemisorption of $[Rh(CO)_2(acac)]$ on TiO_2 calcined at 400 °C and subsequent treatment in CO at 100 °C for 24 h followed by treatment in He at 300 °C for 2 h; and (D) species formed by chemisorption of $[Rh(CO)_2(acac)]$ on TiO_2 calcined at 400 °C and subsequent treatment in CO at 100 °C for 24 h followed by treatment in H_2 at 300 °C for 2 h.

were present in the spectra of the sample formed by deposition of $[Rh_6(CO)_{16}]$ on $TiO_{2,400}$.[28] In contrast, a second Rh−Rh shell ($N = 0.7$, $R = 3.91$ Å), consistent with Rh_6 octahedra ($N_{second-shell} = 1$), was present in the spectra of the sample made with $TiO_{2,200}$. A third Rh−Rh shell ($N = 0.7$, $R = 3.91$ Å) was also present in the spectra of the sample made with $TiO_{2,200}$, indicating that the $[Rh_6(CO)_{16}]$ was significantly aggregated on $TiO_{2,200}$.

The parameters characterizing the Rh-terminal CO contributions in the EXAFS spectra of the samples formed by deposition of $[Rh_6(CO)_{16}]$ on each TiO_2 support are nearly the same as those expected on the basis of X-ray diffraction (XRD) data characterizing crystalline $[Rh_6(CO)_{16}]$ ($Rh-C_{terminal}$: $N = 2$, $R = 1.864$ Å; $Rh-O^*_{terminal}$: $N = 2$, $R = 3.019$ Å),[29] as follows: the $Rh-(CO)_{terminal}$ contributions characterizing the clusters on $TiO_{2,200}$ consist of $Rh-C_{terminal}$ with a coordination number of 2.0 at a distance of 1.87 Å and $Rh-O^*_{terminal}$ with a coordination number of 2.3 at a distance of 2.99 Å. The sample supported on $TiO_{2,400}$ was characterized by similar $Rh-(CO)_{terminal}$ contributions, specifically, a $Rh-C_{terminal}$ with a coordination number of 2.3 at a distance of 1.85 Å and $Rh-O^*_{terminal}$ contribution with a coordination number of 2.5 at a distance of 2.99 Å.

The parameters characterizing the carbon of the bridging carbonyl group in the sample supported on $TiO_{2,200}$ ($Rh-C_{bridging}$: $N = 2.4$, $R = 2.19$ Å) are nearly those expected on the basis of XRD data representing $[Rh_6(CO)_{16}]$ ($N = 2$, $R = 2.168$ Å).[29] In contrast, the data representing the sample supported on $TiO_{2,400}$ are not ($Rh-C_{bridging}$: $N = 3.0$, $R = 2.11$ Å); the $Rh-C_{bridging}$ bonding distance is shorter (by 0.058 Å) and the coordination number larger (by 1.0) than expected for $[Rh_6(CO)_{16}]$. This discrepancy may be explained (a) by interference with a short $Rh-O_{support}$ contribution (not detected in the spectra of this sample, possibly obscured by spectral interference) that may exist at nearly the same distance and (b) by the difficulty in analyzing low-Z contributions by metal-edge EXAFS spectroscopy.[4] It was not possible to characterize the $Rh-O^*_{bridging}$ contributions of the samples formed by deposition of $[Rh_6(CO)_{16}]$ on TiO_2, expected on the basis of XRD data characterizing $[Rh_6(CO)_{16}]$ ($N = 2$, $R = 3.100$ Å),[29] possibly because of interference by other contributions (e.g., $Rh-O^*_{terminal}$).

The only Rh-support contribution found for the samples formed by deposition of $[Rh_6(CO)_{16}]$ represents the sample supported on $TiO_{2,200}$, namely, a short Rh−O contribution ($N = 0.9$, $R = 2.12$ Å). Because the $[Rh_6(CO)_{16}]$ was aggregated, the area of its interface with the support was less than that of site-isolated $[Rh_6(CO)_{16}]$, and some of the Rh-support contributions were evidently small enough to fall below the detection limit. The $[Rh_6(CO)_{16}]$ aggregates on $TiO_{2,400}$ appear to be smaller than those on $TiO_{2,200}$ (as shown by the Rh−Rh shells noted above), but they have smaller cluster-support interface contributions, indicating that the $[Rh_6(CO)_{16}]$ aggregates on $TiO_{2,400}$ are more three-dimensional in character than those on $TiO_{2,200}$, which might be raft-like.

In summary, deposition of $[Rh_6(CO)_{16}]$ from solution gave aggregates on TiO_2 rather than site-isolated $[Rh_6(CO)_{16}]$.

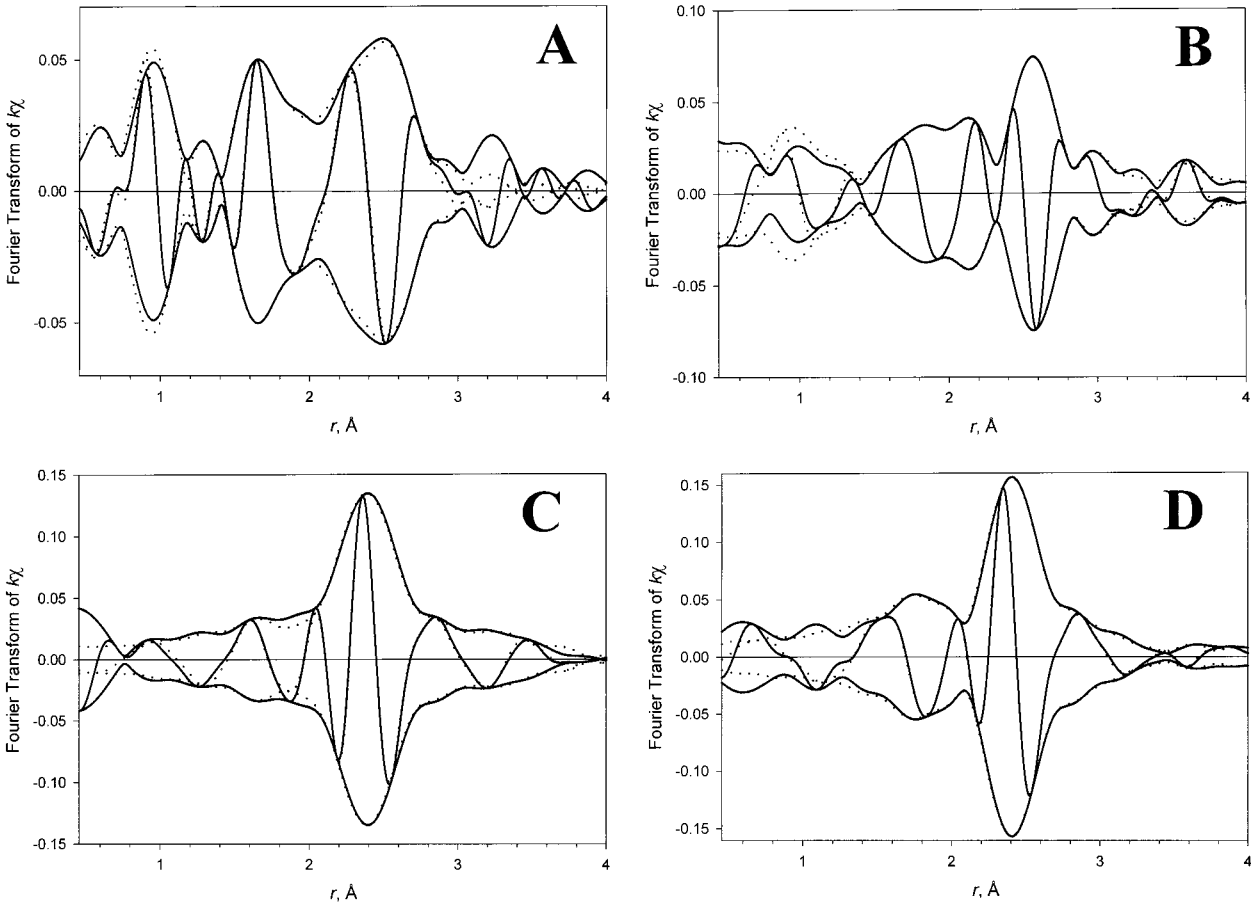

Figure 6. Results of EXAFS data analysis for TiO_2-supported rhodium carbonyls and surface species formed by decarbonylation of rhodium carbonyls: imaginary part and magnitude of the k^1-weighted Fourier transform of raw data (solid lines) and calculated contributions (dotted lines) according to the reported structural parameters. (A) Species formed by chemisorption of $[Rh(CO)_2(acac)]$ on TiO_2 calcined at 400 °C (Δk = 4.25−14.75 Å^{-1}); (B) species formed by chemisorption of $[Rh(CO)_2(acac)]$ on TiO_2 calcined at 400 °C and subsequent treatment in CO at 100 °C for 24 h (Δk = 4.24−14.68 Å^{-1}); (C) species formed by chemisorption of $[Rh(CO)_2(acac)]$ on TiO_2 calcined at 400 °C and subsequent treatment in CO at 100 °C for 24 h followed by treatment in He at 300 °C for 2 h (Δk = 4.21−14.52 Å^{-1}); and (D) species formed by chemisorption of $[Rh(CO)_2(acac)]$ on TiO_2 calcined at 400 °C and subsequent treatment in CO at 100 °C for 24 h followed by treatment in H_2 at 300 °C for 2 h (Δk = 3.58−14.59 Å^{-1}).

Consequently, a separate preparation method was used to form site-isolated $[Rh_6(CO)_{16}]$, as described below.

Site-Isolated $Rh(CO)_2$ on TiO_2 formed from $[Rh(CO)_2(acac)]$. In the following section we summarize evidence that each sample formed by chemisorption of $[Rh(CO)_2(acac)]$ on TiO_2 incorporated predominantly site-isolated rhodium dicarbonyl complexes (which have also been prepared on single crystals of TiO_2 by other means[30]). The numbers of ν_{CO} peaks in the infrared spectra (2) and their positions (2083, 2004 cm^{-1} and 2091, 2017 cm^{-1} in the spectra of the samples supported on $TiO_{2,200}$ (Figure 3) and $TiO_{2,400}$ (Figure 4), respectively) are consistent with reports of supported rhodium dicarbonyls (e.g., 2092, 2014 cm^{-1} for $Rh(CO)_2$ on γ-Al_2O_3 calcined at 400 °C[31] and 2082, 2014 cm^{-1} for $Rh(CO)_2$ on zeolite NaY calcined at 200 or 300 °C,[8] Table 2). The ν_{CO} peaks in the infrared spectrum of $Rh(CO)_2$ on the more highly dehydroxylated of the TiO_2 samples, $TiO_{2,400}$, occur at approximately 10-cm^{-1} higher frequencies than those of the complex supported on $TiO_{2,200}$. The infrared peaks[25] of $Rh(CO)_2$ on $TiO_{2,200}$ and on $TiO_{2,400}$ are broad, which implies a distribution of bonding sites on the support (Figures 3 and 4).

The EXAFS data characterizing the samples formed by chemisorption of $[Rh(CO)_2(acac)]$ (Figures 5 and 6) include no Rh−Rh contributions, consistent with the absence of rhodium clusters or crystallites or aggregates of complexes such as $[Rh(CO)_2(acac)]$.

The Rh−C and Rh−O* contributions (Table 4) confirm the infrared evidence of rhodium dicarbonyl groups in each sample, i.e., coordination numbers of about 2 and bond distances consistent with terminally bonded CO ligands. Specifically, the sample made from $TiO_{2,200}$ is characterized by a Rh−C contribution at 1.86 Å with a coordination number of 1.9 and a Rh−O* contribution at 2.97 Å with a coordination number of 1.7. The sample made with $TiO_{2,400}$ is similarly characterized by a Rh−C contribution at 1.88 Å with a coordination number of 2.0 and a Rh−O* contribution at 3.03 Å with a coordination number of 2.0.

The EXAFS data show how $Rh(CO)_2$ is bonded to the TiO_2. On $TiO_{2,200}$, $Rh(CO)_2$ is bonded to approximately two support oxygen atoms (N = 2.1, with a typical Rh−O distance of 2.07 Å). A Rh−Ti contribution was found with a coordination number of 1.5 at a distance of 2.82 Å. Similarly, a (smaller) Rh−Ti contribution (N = 0.5, R = 2.89 Å) was observed for $Rh(CO)_2$ on $TiO_{2,400}$. The latter sample is characterized by a Rh−O contribution at 2.04 Å with a coordination number of 2.4, which suggests the average of $Rh(CO)_2$ coordinated to two different bonding sites, one with two oxygen atoms and the other with three. However, this suggestion is tentative because the uncertainties in the data may be as large as ±1 for the coordination number and ±0.1 Å for the bond distance.[4]

Site-Isolated $[Rh_6(CO)_{16}]$ formed from $Rh(CO)_2$ on TiO_2. Treatment of the samples formed by chemisorption of $[Rh(CO)_2$-

TABLE 4: XRD and EXAFS Parameters Characterizing Unsupported and TiO_2-Supported Rhodium Carbonyls

XRD parameters			EXAFS parameters determined from the Rh K Edge								
			sample formed from chemisorption of $[Rh(CO)_2(acac)]$ on $TiO_{2,200}$					sample formed from chemisorption of $[Rh(CO)_2(acac)]$ on $TiO_{2,400}$				
$[Rh_6(CO)_{16}]$												
distance[a]	N	R (Å)	backscatterer (shell)	N	R (Å)	$10^3 \times \Delta\sigma^2$ (Å^2)	ΔE_0 (eV)	CO treatment conditions[b]	backscatterer (shell)	N	R (Å)	$10^3 \times \Delta\sigma^2$ (Å^2)	ΔE_0 (eV)
Rh−Rh	4	2.776	CO					no treatment	CO				
1st shell									C	2.0	1.88	−1.82	−20.00
2nd shell	1	3.926	C	1.9	1.86	−2.37	−9.47		O*	2.0	3.03	1.93	−3.95
Rh−CO			O*	1.7	2.97	4.08	−11.47		support				
Rh−C_t	2	1.864	support						O	2.4	2.04	2.19	0.03
Rh−O_{t*}	2	3.019	O	2.1	2.07	−0.90	−3.14		Ti	0.5	2.89	0.44	−16.70
Rh−C_{fb}	2	2.168	Ti	1.5	2.82	5.34	3.06						
Rh−O_{fb*}	2	3.100						100 °C for 1 day	Rh				
			Rh						(1st)	4.1	2.73	1.24	−1.50
			(1st)	4.1	2.75	1.57	2.14		(2nd)	0.9	3.88	6.65	2.37
			(2nd)	0.7	3.88	5.81	1.38		CO				
			CO						terminal				
			terminal						C	2.1	1.84	−0.10	−0.43
			C	1.9	1.85	2.63	−1.20		O*				
			O*	1.9	3.01	−1.57	−0.39		bridging				
			bridging						C	2.2	2.17	−1.00	7.52
			C	1.6	2.17	11.09	−5.41		O*	4.2	3.18	3.58	19.85
			O*	1.6	3.17	2.16	2.96		support				
			support						O	1.4	2.03	−1.85	−8.68
			O	0.5	2.08	−3.35	−1.81		Ti	1.3	2.72	2.01	16.44
			Ti	0.9	2.89	0.86	−16.98						

[a] The subscripts t and fb refer to terminal and face-bridging, respectively. [b] The treatment conditions refer to the samples referred to in the columns both to the right and to the left of the column stating the treatment conditions.

(acac)] on TiO_2 with CO at 100 °C for 1 day converted the surface species predominantly into $[Rh_6(CO)_{16}]$. $[Rh_6(CO)_{16}]$ was extracted from the surface intact into THF, as shown by the infrared spectra of the extract solutions; the spectra of the clusters extracted from $TiO_{2,200}$ (2075 vs, 2043 w, 1808 m cm^{-1} and) and from $TiO_{2,400}$ (2076 vs, 2043 w, 1809 m cm^{-1}) essentially match those of $[Rh_6(CO)_{16}]$ in THF (Figure 1). No other species were extracted from the TiO_2. $[Rh_6(CO)_{16}]$ was also extracted into solutions of [PPN]Cl in THF, as shown by infrared spectra that are nearly identical to that of $[Rh_6(CO)_{16}]$ dissolved in [PPN]Cl in THF (Table 2, Figure 2).[32]

The infrared spectrum[25] of the solid samples made from $TiO_{2,200}$, prior to extraction (2086 vs, 2032 m-sh, 2020 s, 1847 w-sh, 1828 m cm^{-1}, Figure 3), and that made from $TiO_{2,400}$ (2118 vw, 2078 vs, 2050 m-sh, 2013 s, (1990 sh), 1846 w-sh, 1827 m, 1702 m cm^{-1}, Figure 4) are similar to that of $[Rh_6(CO)_{16}]$ in KBr and in THF solution, with the ν_{CO} bands shifted and broadened (and to some extent split) relative to those of $[Rh_6(CO)_{16}]$ in solution, as expected for the oxide-supported species.

The EXAFS spectra (Figures 5 and 6) confirm the identification of $[Rh_6(CO)_{16}]$ in these samples and provide information about the cluster-support interface. The Rh−Rh contributions (Table 4) consist of a first shell with a coordination numbers of 4.1 and 4.1 and distances of 2.75 and 2.73 Å for the samples supported on $TiO_{2,200}$ and $TiO_{2,400}$, respectively, and a second shell with coordination numbers of 0.7 and 0.9 for the respective samples, each at a distance of 3.88 Å. The Rh−Rh first-shell parameters are the same, within the typical experimental uncertainties, as those expected for crystalline $[Rh_6(CO)_{16}]$ (Table 4).[29] The second-shell Rh−Rh parameter values are slightly less the XRD values for $[Rh_6(CO)_{16}]$; however, the Rh−Rh distances of the second Rh−Rh shells are, within the uncertainty of the measurement, multiples of $\sqrt{2}$ of the first-shell Rh−Rh distances measured by EXAFS spectroscopy, as expected for an octahedral metal frame. The fact that the Rh−Rh second-shell coordination numbers are slightly less than the crystallographic value for the Rh_6 octahedron may be the result of interference from other coordination shells (e.g., Rh−support shells), and/or the diminished accuracy of EXAFS spectroscopy in characterizing absorber−backscatterer shells at relatively long distances as a consequence of extinction of the ejected photoelectron.

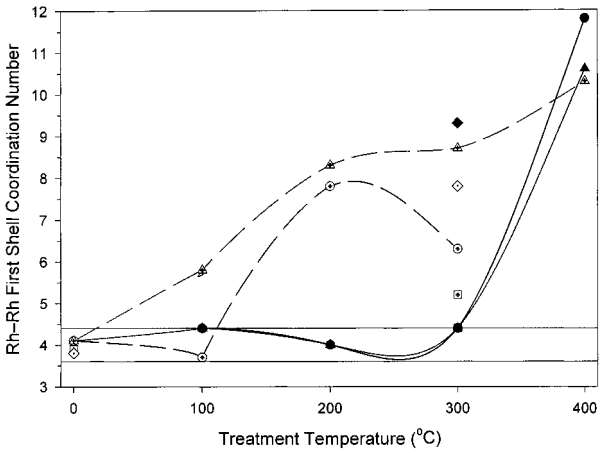

Figure 7. Effect of thermal treatment and TiO_2 support calcination temperature on rhodium cluster stability as shown by the value of the Rh−Rh first-shell coordination number. The horizontal lines mark the region, taking into account the typical EXAFS error estimates, that are consistent with the existence of rhodium octahedra ($N = 4$). Samples treated in He are denoted with solid lines and solid symbols. Samples treated in H_2 are denoted with dashed lines and symbols with a cross inside them. Circles: species formed by chemisorption of $[Rh(CO)_2(acac)]$ on TiO_2 calcined at 400 °C and subsequent treatment in CO at 100 °C for 24 h. Triangles: species formed by chemisorption of $[Rh(CO)_2(acac)]$ on TiO_2 calcined at 200 °C and subsequent treatment in CO at 100 °C for 24 h. Squares: species formed by deposition of $[Rh_6(CO)_{16}]$ on TiO_2 calcined at 400 °C. Diamonds: species formed by deposition of $[Rh_6(CO)_{16}]$ on TiO_2 calcined at 200 °C.

The Rh−CO contributions characterizing these supported samples are also consistent with $[Rh_6(CO)_{16}]$. The clusters

TABLE 5: EXAFS Parameters Characterizing TiO_2-Supported Rhodium Clusters Formed by Thermal Treatment of TiO_2-Supported $[Rh_6(CO)_{16}]$ Formed by CO Treatment at 100 °C for 1 day of the Sample Resulting from Chemisorption of $[Rh(CO)_2(acac)]$ on $TiO_{2,200}$

treatment gas										
helium						hydrogen				
backscatterer (shell)	N	R (Å)	$10^3 \times \Delta\sigma^2$ (Å^2)	ΔE_0 (eV)	treatment temp (°C)	backscatterer (shell)	N	R (Å)	$103 \times \Delta\sigma^2$ (Å^2)	ΔE_0 (eV)
Rh					100	Rh				
(1st)	4.4	2.71	4.42	3.46		(1st)	5.8	2.69	1.96	−1.42
						(2nd)	2.7	3.78	11.35	−1.70
						(3rd)	2.3	4.63	4.28	4.25
CO						residualCO				
terminal						terminal				
C	1.4	1.84	4.22	−6.25		C	0.9	1.86	−3.34	0.00
bridging										
C	0.9	2.14	−3.66	0.97						
O*	1.6	3.15	6.77	4.73						
support						support				
O	1.3	2.03	1.62	−13.24		O	1.2	2.02	−2.68	−6.19
Ti	1.1	2.85	1.19	−8.43		Ti	1.5	3.08	7.08	−4.72
Rh					200	Rh				
(1st)	4.0	2.65	3.32	4.24		(1st)	8.3	2.67	2.53	−0.09
(2nd)	0.9	3.72	10.90	1.52		(2nd)	1.4	3.80	4.78	−8.50
						(3rd)	1.9	4.63	1.95	2.94
residual CO										
bridging										
C	0.7	2.18	−6.43	0.03						
support						support				
O	1.4	2.04	−3.12	−14.45		O	0.3	2.15	−5.76	−16.96
Ti	0.8	2.84	6.13	−0.16		Ti	0.7	3.12	1.75	−10.86
Rh					300	Rh				
(1st)	4.4	2.64	2.39	3.81		(1st)	8.7	2.66	2.73	2.90
(2nd)	1.0	3.82	8.02	−6.79		(2nd)	5.4	3.74	13.39	0.79
						(3rd)	2.8	4.64	3.36	1.69
residual CO										
bridging										
C	0.3	2.18	−8.21	17.00						
support						support				
O	1.1	2.11	−2.63	−14.77		O	0.4	2.06	1.65	−17.85
Ti	0.8	2.97	5.44	−3.32		Ti	0.3	3.10	0.97	−2.68
Rh					400	Rh				
(1st)	10.6	2.64	2.36	2.29		(1st)	10.3	2.66	3.41	−2.47
(2nd)	2.3	3.72	8.53	−1.05		(2nd)	5.0	3.75	13.97	−4.84
(3rd)	5.8	4.60	6.26	1.94		(3rd)	3.0	4.63	3.89	−3.97
support						support				
Ti	0.4	2.72	1.50	−0.52		Ti	1.1	3.08	2.47	−2.84

supported on $TiO_{2,200}$ are characterized by all four Rh−CO contributions expected for $[Rh_6(CO)_{16}]$ with parameter values that match, within the expected experimental uncertainty, the XRD values for $[Rh_6(CO)_{16}]$ (Table 4). The clusters supported on $TiO_{2,400}$ are also characterized by Rh−C contributions (Table 4) matching those of $[Rh_6(CO)_{16}]$, but the nearly equal distances and similar phases of the two Rh−O* contributions (from the terminal and bridging CO ligands) make it difficult to separate these contributions. Consequently, a single broad Rh−O* contribution, representing a superposition of the Rh−O*$_t$ and Rh−O*$_b$ contributions (where the subscripts represent terminal and bridging, respectively), was used to fit the Rh−O* contributions (Table 4).

The interface between $[Rh_6(CO)_{16}]$ and TiO_2 for each sample is characterized by a short Rh−O contribution and a Rh−support-layer Ti contribution. The Rh−O (R = 2.08 Å) and Rh−Ti (R = 2.89 Å) contributions representing the clusters on $TiO_{2,200}$ occur in nearly a 1:2 ratio (N_{Rh-O} = 0.5, N_{Rh-Ti} = 0.9), which suggests distortion of the clusters relative to those in the crystalline state and bonding to a surface face with a stoichiometry similar to that of bulk TiO_2. However, we suggest that the bonding of $[Rh_6(CO)_{16}]$ to $TiO_{2,400}$ may occur at different sites, because the Rh−O (R = 2.03 Å) and Rh−Ti (R = 2.72 Å) contributions occur in essentially a 1:1 ratio (N_{Rh-O} = 1.4, N_{Rh-Ti} = 1.3). We emphasize that these suggestions are only tentative because the experimental uncertainty in the EXAFS data makes characterizing the cluster-support interface difficult.

Decarbonylation of TiO_2-Supported $[Rh_6(CO)_{16}]$ Aggregates. The ν_{CO} peaks characterizing $[Rh_6(CO)_{16}]$ deposits on TiO_2 disappeared as a result of heating the sample to 300 °C in either in He or H_2. The EXAFS structural parameters characterizing these decarbonylated samples (Table 3 and Figure 7) indicate sintering to give particles (crystallites) of rhodium. Sintering occurred to a greater extent on $TiO_{2,200}$ (which has a relatively high surface water content) than on $TiO_{2,400}$, as evidenced by the higher Rh−Rh coordination numbers representing the former. Specifically, the rhodium particles on $TiO_{2,200}$ formed by treatments in He and H_2 at 300 °C are characterized by four Rh−Rh shells and first-shell coordination numbers of 9.3 and 7.5, respectively. The rhodium particles are roughly 25 and 14 Å in average diameter, respectively, as estimated by the model of Kip et al.[33] The rhodium particles

TABLE 6: EXAFS Parameters Characterizing TiO_2-Supported Rhodium Clusters Formed by Thermal Treatment of TiO_2-Supported $[Rh_6(CO)_{16}]$ Formed by CO Treatment at 100 °C for 1 day of the Sample Resulting from Chemisorption of $[Rh(CO)_2(acac)]$ on $TiO_{2,400}$.

treatment gas										
helium						hydrogen				
backscatterer (shell)	N	R (Å)	$10^3 \times \Delta\sigma^2$ (Å^2)	ΔE_0 (eV)	treatment temp (°C)	backscatterer (shell)	N	R (Å)	$10^3 \times \Delta\sigma^2$ (Å^2)	ΔE_0 (eV)
Rh					100	Rh				
(1st)	4.4	2.79	8.37	−10.83		(1st)	3.7	2.68	4.45	3.46
						(2nd)	0.6	3.87	4.26	2.54
CO						residual CO				
terminal										
C	0.3	1.87	−7.76	−18.11						
O*	0.6	2.97	−6.87	15.52						
						bridging				
						C	0.9	2.02	−0.34	−12.57
support						support				
O	2.0	2.02	0.21	0.73						
Ti	1.3	2.87	0.19	−19.52		Ti	1.1	2.79	6.87	−9.79
						O	0.6	3.57	−7.31	−18.33
Rh					200	Rh				
(1st)	4.0	2.66	1.33	−1.87		(1st)	7.8	2.63	4.38	4.29
(2nd)	1.2	3.75	8.27	−3.06		(2nd)	1.9	3.63	10.74	3.09
support						support				
O	1.9	2.03	9.52	−3.59						
Ti	1.0	2.96	3.57	3.34		Ti	0.7	2.72	2.11	−0.78
O	1.9	3.41	−0.36	−3.08						
Rh					300	Rh				
(1st)	4.4	2.63	1.55	8.48		(1st)	6.3	2.64	3.11	1.25
(2nd)	1.0	3.60	3.80	12.34		(2nd)	1.7	3.69	9.35	−1.35
						(3rd)	1.6	4.62	9.62	0.20
support						support				
O	0.9	2.01	8.63	3.77		O	0.4	2.13	0.36	−17.89
Ti	0.8	2.97	4.62	−17.40		Ti	0.5	3.42	1.64	−0.90
O	1.3	3.37	−7.15	−4.88						
Ti	0.6	4.01	1.19	2.22						
Rh					400					
(1st)	11.8	2.65	5.74	4.50						
(2nd)	2.0	3.75	13.51	−6.57						
(3rd)	2.9	4.64	8.33	−2.04						
support										
Ti	1.1	2.85	1.04	−16.49						
O	2.9	3.48	1.42	−12.44						

supported on $TiO_{2,400}$ formed by treatment in He and H_2 at 300 °C are characterized by Rh−Rh shells and first-shell coordination numbers of 4.1 and 5.2, respectively. The particles are roughly 8 and 9 Å in average diameter, respectively, as estimated by the model stated above.

In summary, $[Rh_6(CO)_{16}]$ deposited on TiO_2 and treated in He or H_2 gives metal particles and not site-isolated Rh_6. We infer that the initial presence of aggregates of $[Rh_6(CO)_{16}]$ facilitates sintering of the metal upon removal of the CO ligands.

Formation of Site-Isolated Rh_6 from $[Rh_6(CO)_{16}]$ on TiO_2. When site-isolated $[Rh_6(CO)_{16}]$ on TiO_2 was treated at 300 °C in He or H_2, the CO ligands were removed, as shown by the disappearance of the ν_{CO} bands in the infrared spectrum. The EXAFS results (Figures 5 and 6) are consistent with this conclusion; results tracking the changes as the CO ligands were removed are summarized in Tables 5 and 6 and Figure 7.

Treatment of $TiO_{2,200}$-supported $[Rh_6(CO)_{16}]$ in H_2, even at temperatures as low as 100 °C, led to sintering, as shown by the presence of three or more Rh−Rh shells in the EXAFS spectra. The degree of sintering, indicated by the Rh−Rh coordination numbers, increased with increasing treatment temperature (Figure 7). In contrast, $[Rh_6(CO)_{16}]$ on $TiO_{2,400}$ was resistant to sintering in H_2. The Rh−Rh contributions (first shell, $N = 3.7$, $R = 2.68$ Å; second shell, $N = 0.6$, $R = 3.87$ Å) and the Rh−Ti contribution ($N = 1.1$, $R = 2.79$ Å) characterizing the sample after treatment in H_2 at 100 °C show that the octahedral cluster frame was essentially retained. The EXAFS data indicate some carbon remaining on the clusters (Rh−C: $N = 0.9$, $R = 2.02$ Å), identified by the phase of the backscatterer, possibly from residual CO[34] associated with the Rh_6. Treatment of the sample supported on $TiO_{2,400}$ in H_2 at higher temperatures (200 and 300 °C), however, led to removal of the carbon (no Rh−C contributions were observed in the EXAFS spectra), accompanied by sintering of the rhodium to form particles, as shown by the Rh−Rh coordination numbers (Table 6); a third Rh−Rh shell at 4.62 Å appeared after the treatment at 300 °C. The average rhodium particle diameter was approximately 11−15 Å after treatment in He at either 200 or 300 °C.[35]

In contrast to the treatments in H_2, treatment in He at temperatures up to 300 °C did not cause sintering of the rhodium as the CO ligands were removed. Following treatment with He at temperatures up to 300 °C, the cluster frames remained essentially intact, as shown by the almost unchanged Rh−Rh contributions (Tables 5 and 6). The Rh−Rh first-shell coordination numbers ($N = 4.4$, 4.0, and 4.4 characterizing the sample supported on $TiO_{2,200}$ and $N = 4.4$, 4.0, and 4.4 characterizing the sample supported on $TiO_{2,400}$ resulting from treatments in He at 100, 200, and 300 °C, respectively) show that the supported clusters are well approximated as Rh_6 octahedra. The

second-shell data confirm this conclusion for the sample after treatment in He at 200 °C ($N_{second-shell}$: 0.9 and 1.2 for the samples made from $TiO_{2,200}$ and $TiO_{2,400}$, respectively) and at 300 °C ($N_{second-shell}$: 1.0 and 1.0 for the samples made from $TiO_{2,200}$ and $TiO_{2,400}$, respectively). (The quality of the data characterizing the sample after treatment at 100 °C was not sufficient for isolation of this contribution.)

The stepwise loss of CO ligands as the treatment temperature increased is indicated by the EXAFS data (Tables 5 and 6). Following treatment in He at 100 °C, both the terminal (Rh−C: $N = 1.4$, $R = 1.84$ Å; Rh−O* was not observed) and bridging (Rh−C: $N = 0.9$, $R = 2.14$ Å; Rh−O*: $N = 1.6$, $R = 3.15$ Å) carbonyl contributions of the cluster on $TiO_{2,200}$ were smaller than those of the untreated sample. After treatment in He at 200 °C for 2 h, a small Rh−C contribution ($N = 0.7$), identified by the phase of the backscatterer, at a $Rh-C_{terminal}$ distance ($R = 2.18$ Å, but without a discernible Rh−O* contribution) was observed, indicating that almost all of the CO ligands had been removed. After further treatment in He at 300 °C for 2 h, the Rh−C contribution was reduced ($N = 0.3$, $R = 2.18$ Å), but its continued presence indicates that the rhodium clusters on $TiO_{2,200}$, although free of carbonyl ligands, were not completely bare−they still had some nonsupport ligands, indicated by the Rh−C contribution.

The spectrum of the sample made from site-isolated $[Rh_6(CO)_{16}]$ on $TiO_{2,400}$ by treatment in He at 100 °C had reduced $Rh-CO_{terminal}$ contributions (Rh−C: $N = 0.3$, $R = 1.87$ Å; Rh−O*: $N = 0.6$, $R = 2.97$ Å), relative to those of the untreated sample, and no bridging carbonyl contributions. After treatment in He at temperatures ≥ 200 °C, no carbonyl or residual carbon contributions remained, consistent with the identification of the surface species as bare, site-isolated hexarhodium clusters anchored to the support (Table 6).

The Rh−Rh bond lengths tended to decrease, as expected, as the clusters were transformed from coordinatively saturated TiO_2-supported $[Rh_6(CO)_{16}]$ ($R = 2.75$ and 2.73 Å for the samples supported on $TiO_{2,200}$ and $TiO_{2,400}$, respectively) to coordinatively unsaturated hexarhodium octahedra with only the support (and possibly some residual carbon) as ligands ($R = 2.71$ and 2.79 Å; $R = 2.65$ and 2.67 Å; and $R = 2.64$ and 2.66 Å for the samples supported on $TiO_{2,200}$ and $TiO_{2,400}$ following He treatment at 100, 200, and 300 °C, respectively).

Treatment of these samples in He at a higher temperature, 400 °C, for 2 h led to substantial sintering to give relatively large rhodium particles, as shown by the three Rh−Rh shells and Rh−Rh first-shell coordination numbers approaching the limiting value of 12 for bulk rhodium (i.e., $N_{first-shell} = 10.6$ and 11.8 for the samples supported on $TiO_{2,200}$ and $TiO_{2,400}$, respectively).

Characterization of the Metal-Support Interface during Formation of Site-Isolated Rh_6 from $[Rh_6(CO)_{16}]$ on TiO_2. EXAFS data characterizing the metal−support interface are most accurate when supported metals are well-defined structurally and maximally dispersed; in this sense, the site-isolated Rh_6 clusters on TiO_2 are prototypes. The cluster-$TiO_{2,200}$ interfaces are characterized by a Rh−O bonding contribution ($N = 1.3$, 1.4, and 1.1 and $R = 2.03$, 2.04, and 2.11 Å following treatments in He at 100, 200, and 300 °C, respectively) that demonstrates a nearly a one-to-one Rh-to-oxygen stoichiometry. The Rh−Ti contributions ($N = 1.1$, 0.8, and 0.8 and $R = 2.85$, 2.84, and 2.97 Å following treatments in He at 100, 200, and 300 °C, respectively) are taken as evidence of titanium in a subsurface layer of the support.

In contrast, the site-isolated hexarhodium clusters on $TiO_{2,400}$ formed in He at 100 °C are characterized by a Rh−O bonding contribution ($N = 2.0$, $R = 2.02$ Å) with nearly a 2:1 stoichiometry. Thus, the Rh-support contributions characterizing the clusters on $TiO_{2,400}$ imply binding to a TiO_2 face or faces (or surface defects) different from those of $TiO_{2,200}$. Again, a Rh−Ti contribution ($N = 1.3$, $R = 2.87$ Å) indicates titanium in a subsurface layer of the support. Following further treatment in He at 200 °C, the sample supported on $TiO_{2,400}$ was still represented by a Rh−O bonding contribution ($N = 1.9$, $R = 2.03$ Å) indicating nearly a 2:1 Rh-to-oxygen stoichiometry, still with a Rh−Ti contribution ($N = 1.0$, $R = 2.96$ Å), and there was an additional contribution, which is tentatively assigned to an oxygen backscatterer from another subsurface support layer (Rh−O: $N = 1.9$, $R = 3.41$ Å).[36] The Rh−O bonding contribution changed following further treatment in He at 300 °C to indicate a nearly 1:1 Rh-to-oxygen stoichiometry (Rh−O: $N = 0.9$, $R = 2.01$ Å); there was still a Rh−Ti contribution: $N = 0.8$, $R = 2.97$ Å. The sample supported on $TiO_{2,400}$ following treatment in He at 300 °C is also characterized by two additional small contributions that are tentatively assigned to subsurface support layers, another Rh−O shell ($N = 1.3$, $R = 3.37$ Å)[36] and another Rh−Ti shell ($N = 0.6$, $R = 4.01$ Å).[36] The significance of the changes is unclear in view of the uncertainty in the multiple-shell data characterizing the metal−support interface.[4]

Discussion

Chemistry of Rhodium Carbonyls on TiO_2 Parallels that in Neutral Solutions. Chini and Martinengo[37] demonstrated reactions of rhodium carbonyls to give anionic rhodium carbonyls in basic solutions and neutral rhodium carbonyls in neutral solutions. For example, in methanol, $[Rh(CO)_2Cl]_2$ reacts with H_2O and CO to form $[Rh_4(CO)_{12}]$ and $[Rh_6(CO)_{16}]$:[37]

$$2[Rh(CO)_2Cl]_2 + 6CO + 2H_2O \rightarrow [Rh_4(CO)_{12}] + 2CO_2 + 4HCl \quad (1)$$

$$3[Rh(CO)_2Cl]_2 + 7CO + 3H_2O \rightarrow [Rh_6(CO)_{16}] + 3CO_2 + 6HCl \quad (2)$$

Rh(I) dicarbonyls on TiO_2 were converted into neutral rhodium carbonyl clusters, $[Rh_6(CO)_{16}]$, when they reacted with surface water and CO, which suggests that the TiO_2 surface provides a medium for chemistry similar to that of a neutral solution.

Chemistry of Rhodium Carbonyls on TiO_2 Parallels that on other Neutral Surfaces. With extensive infrared analysis, but limited precautions taken for air sensitivity, Evans and McNulty[38] observed the intraconversion of $[Rh_4(CO)_{12}]$ and $[Rh_6(CO)_{16}]$ and their conversion into rhodium subcarbonyls on supports represented as neutral, Al_2O_3 and TiO_2. $[Rh(CO)_2(acac)]$ was converted into $[Rh_6(CO)_{16}]$ by reductive carbonylation in the pores of zeolite NaY, also represented as neutral.[8] $[Rh_6(CO)_{16}]$ was formed in the pores of zeolites,[39−42] from chloride salts of rhodium; reduction with CO converted Rh(III) to Rh(I) complexes and finally $[Rh_6(CO)_{16}]$; the presence of water is thought to be essential for the final reduction step.[42−44] All of these results reinforce the inference that neutral rhodium carbonyl clusters form on surfaces that can be described as neutral.

Our results agree with previous results[8] showing that $[Rh(CO)_2(acac)]$ is a good precursor for the synthesis of site-isolated $[Rh_6(CO)_{16}]$ on supports; this precursor offers the advantage that chloride or other anions, which would remain adsorbed on the support after the synthesis, are avoided.[45] The chemistry of

rhodium carbonyls on TiO_2 is also similar to that of iridium carbonyls on TiO_2.[46]

Metal Carbonyls as Probes of Support Surface Chemistry. The interactions of a metal carbonyl with a metal oxide or zeolite surface can be a sensitive probe of the acid−base character of the surface. The acid−base properties of a support may be diagnosed by the identification of the metal carbonyl clusters formed, for example, by reductive carbonylation of metal complex and/or deposition of a metal carbonyl cluster.[47,48] When the surface species on a family of variously treated supports such as those considered in this work are structurally equivalent (in our case, $Rh(CO)_2$), the ν_{CO} positions may be diagnostic of the acid−base character of the support (Table 2). Within the resolution of the spectrometer, the ν_{CO} positions of $Rh(CO)_2$ on $TiO_{2,400}$ match those of this complex on γ-Al_2O_3 calcined at 400 °C,[31] which implies similar surface chemistry for γ-Al_2O_3 and TiO_2. The antisymmetric ν_{CO} mode position is essentially the same for the complex on zeolite NaY calcined at 200 or 300 °C[8] as for the complex on either γ-Al_2O_3 or TiO_2, but the symmetric ν_{CO} mode position of $Rh(CO)_2$ on zeolite NaY matches that of the complex on the more basic zeolite NaX calcined at 300 °C.[9] The data suggest that $TiO_{2,200}$, which has more surface water than TiO_2 calcined at higher temperatures, probably has a slightly more basic surface than $TiO_{2,400}$, as both the symmetric and antisymmetric modes of anchored $Rh(CO)_2$ are virtually the same as those of this complex on the basic zeolite NaX calcined at 300 °C.[9]

Neutral surfaces such as those of zeolite NaY[8] calcined at 200 or 300 °C, γ-Al_2O_3 calcined at 400 °C,[31] or $TiO_{2,400}$ lead to the formation of $[Rh_6(CO)_{16}]$ from supported $Rh(CO)_2$ in the presence of CO at temperatures ≥ 100 °C. The reductive carbonylation of $Rh(CO)_2$ supported on $TiO_{2,200}$, which appears to be more basic than the three other supports referred to immediately above, also gives $[Rh_6(CO)_{16}]$, which implies that the surface chemistry of mildly calcined TiO_2 is on the borderline between neutral and basic (and depends on how acidity is measured). In contrast, the more basic zeolite NaX gives anions, $[Rh_6(CO)_{15}]^-$, from supported $Rh(CO)_2$ under CO at 125 °C.[9]

On the basis of a comparison of the ν_{CO} positions of supported $Rh(CO)_2$ and the products of reductive carbonylation, we propose the following list of relative base strengths (from neutral to the most basic in character) for these surfaces: γ-$Al_2O_{3,400}$ ≈ $TiO_{2,400}$ < $(\text{zeolite NaY})_{200}$ ≈ $(\text{zeolite NaY})_{300}$ < $TiO_{2,200}$ < $(\text{zeolite NaX})_{300}$.

Decarbonylation of TiO_2-Supported $[Rh_6(CO)_{16}]$ and Formation of Carbon-Containing Ligands on the Clusters. The removal of CO from metal oxide supported metal carbonyl clusters has been inferred to involve surface water (and/or OH groups) of the support and C−O bond-breaking,[49] the latter indicated by the formation of CO_2 as a product.[50] Thus, we suggest that decarbonylation of TiO_2-supported rhodium carbonyl clusters also involves C−O bond breaking and that the products may include carbon or carbon-containing species on the clusters, consistent with the EXAFS results. The carbon or carbon-containing species are bonded to the clusters at a Rh−C distance intermediate between those typical of $Rh-C_{terminal}$ and $Rh-C_{bridging}$ in rhodium carbonyls. Further decarbonylation in H_2 at higher temperatures leads to removal of the carbon-containing species and sintering of the rhodium (Table 6). The carbon or carbon-containing species may help to stabilize the supported Rh_6 clusters.[51] After treatment in He at 400 °C, the carbon-containing species were no longer detected in the EXAFS spectrum of the clusters on $TiO_{2,200}$, likely having desorbed or reacted, and the Rh_6 octahedra−now approximated as bare except for the support ligand−were no longer so resistant to sintering on the TiO_2.

Although no Rh−C contributions were detected in the EXAFS spectra of Rh_6 on $TiO_{2,400}$, we cannot (because of the uncertainties in the EXAFS data) rule out the possibility that these clusters retained some nonsupport ligands. The Rh−Rh distances determined by EXAFS spectroscopy of the sample decarbonylated in He at 300 °C are only a few hundredths of an angstrom shorter than those of fully coordinated bulk rhodium metal. Theoretical results show that significantly shorter (by about of 0.1−0.2 Å) metal−metal bond distances relative to the bulk metal are expected for bare metal clusters of low nuclearity (4−6 atoms) bonded to a zeolite[52] or MgO.[53] Consequently, we infer that strong bonding of Rh_6 to the support (such as at highly unsaturated defect sites)[53] and/or undetected ligands may account for the Rh−Rh distance.

Influence of the Metal-Support Interface on Stability of Site-Isolated Rh_6. The positions of the terminal ν_{CO} peaks in the infrared spectra of TiO_2-supported site-isolated $[Rh_6(CO)_{16}]$ depend on the support calcination temperature; thus, we infer that the predominant bonding sites for the clusters are different for the two differently calcined supports.

This inference is bolstered by the EXAFS data characterizing the samples prior to and following decarbonylation in He, as follows. The $Rh-O_{support}$ contribution of site-isolated $[Rh_6(CO)_{16}]$ on $TiO_{2,400}$ is larger (the coordination number is 0.9 larger) and characterized by a shorter distance (by 0.05 Å) than the corresponding contribution for site-isolated $[Rh_6(CO)_{16}]$ on $TiO_{2,200}$. Differences in the ratio of the coordination numbers of the Rh−O and Rh−Ti contributions were observed for the samples made with $TiO_{2,200}$ and $TiO_{2,400}$ (1:1 and 2:1, respectively, Tables 5 and 6) after treatment in He at temperatures up to 200 °C; these results confirm the differences in bonding of the rhodium clusters to the differently treated supports.

When decarbonylation was complete, following treatment in He at 300 °C, the coordination numbers of the Rh−O and Rh−Ti contributions became essentially the same for the clusters on the two differently calcined supports. However, comparison of the Rh−O and Rh−Ti distances of the samples before and after decarbonylation suggests different Rh−O−Ti angles, which are indicative of the Rh_6-support bonding. After treatment of the samples in He at 100 °C for 2 h, the Rh−O and Rh−Ti distances were essentially the same for the two samples, implying similar Rh−O−Ti angles. Following the next decarbonylation step (treatment in He at 200 °C), the Rh−O bond distances remained the same, but the Rh−Ti distance representing the sample made with $TiO_{2,400}$ increased by 0.09 Å, whereas that representing the sample made with $TiO_{2,200}$ remained unchanged (Tables 5 and 6). The implication of these results is that the O−Rh−Ti angle stayed the same for the sample supported on $TiO_{2,200}$ but changed for the sample supported on $TiO_{2,400}$ following treatment in He at 200 °C.

After the final decarbonylation step (treatment in He at 300 °C), the Rh−O and Rh−Ti distances remained essentially the same for the sample supported on $TiO_{2,400}$, whereas the Rh−Ti distance representing the sample supported on $TiO_{2,200}$ increased and became the same as that representing the sample supported on $TiO_{2,400}$, and the Rh−O distance of the sample supported on $TiO_{2,200}$ increased to become 0.1 Å longer than that of the sample supported on $TiO_{2,400}$. Hence, although the support coordination numbers were nearly the same for the clusters on the TiO_2 samples calcined at the two temperatures, the O−Rh−Ti angles were different; the results imply that the Rh_6 octahedra

were bound to the different TiO_2 surfaces with different geometries and suggest bonding at different defect sites.

The differences in bonding of Rh_6 to the two TiO_2 surfaces prepared by calcining at two different temperatures are consistent with the role of nonsupport ligands in helping to stabilize the rhodium clusters. The EXAFS data clearly show that the Rh_6 octahedra supported $TiO_{2,200}$ were stabilized by ligands (with a carbon-containing ligand shell centered at a Rh−C distance of about 2.18 Å), whereas such a shell was not found for the Rh_6 octahedra supported on $TiO_{2,400}$, a support to which the clusters were more strongly bound (indicated the resistance to sintering of the clusters and by the Rh−O distance that was 0.1 Å shorter than for the clusters on $TiO_{2,200}$) and in a different geometry (the O−Rh−Ti angle was smaller than for the clusters on $TiO_{2,200}$).

Thus, although the Rh−support interfaces of the fully decarbonylated hexarhodium clusters on TiO_2 are not unambiguously determined by the data, differences in the Rh−support interfaces are clearly shown to arise as a result of support calcination at different temperatures. Thus, the results point to the importance of localized differences in the supports, i.e., defects, influencing the cluster−support bonding. Consequently, we infer that localized defects in the support need to be included in samples−such as single crystals−intended to model technologically useful supported metal catalysts. This need for defects suggests that thin films of TiO_2 grown on a single metal crystal with defects may be a better model of a TiO_2 powder support than single TiO_2 crystals with stable faces.

Conclusions

An efficient method for preparing nearly uniform, site-isolated, and apparently bare octahedral hexarhodium clusters on TiO_2 involves the use of He at 300 °C to decarbonylate site-isolated supported $[Rh_6(CO)_{16}]$ formed by reductive carbonylation (in CO at 1 atm and 100 °C for 1 day) of $[Rh(CO)_2(acac)]$ supported on TiO_2 calcined at 400 °C. The spectroscopic evidence demonstrates a role of the support in forming and stabilizing the Rh_6 octahedra. These Rh_6 octahedra on TiO_2 are among the best-defined site-isolated nanoclusters known. Their bonding to the support is sensitive to the support calcination temperature, which implicates defect sites in the metal−support bonding.

Acknowledgment. This research was supported by the U.S. Department of Energy, Office of Energy Research, Office of Basic Energy Sciences, Division of Chemical Sciences, Contract FG02-87ER13790. We acknowledge the support of the U.S. Department of Energy, Division of Materials Sciences, under Contract Number DE-FG05-89ER45384, for its role in the development and operation of beamline X-11A at the National Synchrotron Light Source (NSLS). A number of the EXAFS experiments were conducted at NSLS, which is supported by the Department of Energy, Division of Materials Sciences and Division of Chemical Sciences, under Contract Number DE-AC02-76CH00016. The remaining EXAFS experiments were performed at the Stanford Synchrotron Radiation Laboratory (SSRL), which is operated by Stanford University for the Department of Energy, Office of Basic Energy Sciences. We thank the staffs of the SSRL and of beam line X-11A at NSLS for their assistance. The EXAFS data were analyzed with XDAP.[14]

Supporting Information Available: Supporting Information Table 1 summarizing the diagnostics analyzing the fitting of the EXAFS data. This material is available free of charge via the Internet at http://pubs.acs.org.

References and Notes

(1) Brown, K.; Tegoni, M., Prudencio, M.; Pereira, A. S.; Besson, S.; Moura, J. J.; Moura, I. Cambillau, C. *Nature Struct. Biol.* **2000**, *7*, 191.

(2) (a) *Oil Gas J.* **1992**, *190*, 29. (b) Miller, J. T.; Meyers, B. C.; Modica, F. S.; Lane, G. S.; Vaarkamp, M.; Koningsberger, D. C. *J. Catal.* **1993**, *143*, 395.

(3) Gates, B. C. *Chem. Rev.* **1995**, *95*, 511.

(4) Goellner, J. F.; Gates, B. C.; Vayssilov, G. N.; Rösch, N. *J. Am. Chem. Soc.* **2000**, *122*, 8056.

(5) (a) Berko, A.; Menesi, G.; Solymosi, F. *J. Phys. Chem.* **1996**, *100*, 17732. (b) Berko, A.; Menesi, G.; Solymosi, F. *Surf. Sci.* **1997**, *372*, 202. (c) Berko, A.; Solymosi, F. *Surf. Sci.* **1998**, *400*, 281.

(6) (a) Valden, M.; Goodman, D. W. *Science* **1998**, *281*, 1647. (b) Xu, C.; Goodman, D. W. *Chem. Phys. Lett.* **1996**, *263*, 13.

(7) Panjabi, G. Ph.D. Dissertation, University of California, Davis, 2000.

(8) Weber, W. A.; Gates, B. C. *J. Phys. Chem. B* **1997**, *101*, 10423.

(9) Weber, W. A.; Phillips, B. L.; Gates, B. C. *Chem. Eur. J.* **1999**, *5*, 2899.

(10) Gates, B. C.; Lamb H. H. *J. Mol. Catal.* **1989**, 52, 1.

(11) Jentoft, R. E.; Deutsch, S. E.; Gates, B. C. *Rev. Sci. Instrum.* **1996**, *67*, 2111.

(12) van Zon, J. B. A. D.; Koningsberger, D. C.; van't Blik, H. F. J.; Sayers, D. E. *J. Chem. Phys.* **1985**, *82*, 5742.

(13) Kirlin, P. S.; van Zon, F. B. M.; Koningsberger, D. C.; Gates, B. C. *J. Phys. Chem.* **1990**, *94*, 8439.

(14) Vaarkamp, M.; Linders, J. C.; Koningsberger, D. C. *Physica B* **1995**, *209*, 159.

(15) Duivenvoorden, F. B. M.; Koningsberger, D. C.; Uh, Y. S.; Gates, B. C. *J. Am. Chem. Soc.* **1986**, *108*, 6254.

(16) (a) Zabinsky, S. I.; Rehr, J. J.; Ankudinov, A.; Albers, R. C.; Eller, M. J. *Phys. Rev. B.* **1995**, *52*, 2995. (b) Ankudinov, A. Ph.D. Dissertation, University of Washington, 1996.

(17) Wycoff, R. W. G., Ed. *Crystal Structures*, 2nd ed.; Wiley: New York, 1963; Vol. 1, p 10.

(18) *Structure Reports* **1964**, *29A*, 130.

(19) van Zon, F. B. M.; Maloney, S. D.; Gates, B. C.; Koningsberger, D. C. *J. Am. Chem. Soc.* **1993**, *115*, 10317.

(20) van Zon, J. B. A. D. Dissertation, Eindhoven University of Technology, The Netherlands, 1988.

(21) van Zon, J. B. A. D.; Koningsberger, D. C.; Gates, B. C. *J. Phys. Chem.* **1985**, *82*, 5742.

(22) Coey, J. M. D. *Acta Crystallogr.* **1970**, *B26*, 1876.

(23) Mason, R.; Rae, A. I. M. *J. Chem. Soc. A* **1968**, 778.

(24) Lytle, F. W.; Sayers, D. E.; Stern, E. A. *Physica B* **1989**, *158*, 701.

(25) The hydroxyl region of the infrared spectrum is broad and muted, preventing a clear and useful analysis of this portion of the spectrum.

(26) Beck, W.; Lottes, K. *Chem. Ber.* **1961**, *94*, 2578.

(27) Vaarkamp, M. *Catal. Today* **1998**, *39*, 271.

(28) The Rh−Rh second shell expected for a Rh_6 octahedron is most likely hidden by destructive interference with other spectral components and noise.

(29) Corey, E. R.; Dahl, L. F.; Beck, W. *J. Am. Chem. Soc.* **1963**, *85*, 1202.

(30) Hayden, B. E.; King, A.; Newton, M. A. *Surf. Sci.* **1998**, *397*, 305.

(31) Goellner, J. F. Ph.D. Dissertation, University of California, Davis, 2000.

(32) When $[Rh_6(CO)_{16}]$ was dissolved in THF containing [PPN]Cl, it reacted to form rhodium carbonyl chlorides. Similarly, $[Rh_6(CO)_{16}]$ extracted from TiO_2 into solutions of [PPN]Cl in THF reacted to form the same rhodium carbonyl chlorides. Thus, the results are consistent with identification of $[Rh_6(CO)_{16}]$ on the TiO_2.

(33) Kip, B. J., Duivenvoorden, M.; Koningsberger, D. C.; Prins, R. *J. Catal.* **1987**, *105*, 26.

(34) Another possibility is that this Rh−C contribution arises from some hydrocarbon formed during the decarbonylation process; the point is addressed in the Discussion section.

(35) The rhodium particles supported on $TiO_{2,\ 400}$ following treatment at 300 °C in H_2 are larger than those formed following treatment at 200 °C in H_2, as demonstrated by an additional Rh−Rh shell characterizing the former sample but not the latter. The flattening of the TiO_2-supported rhodium particles into raft-like structures (which are not well-represented by a particle diameter estimated from Kip's analysis[33]) is indicated by the Rh−Rh first-shell coordination number being smaller (Table 6) for the larger particles formed following treatment at 300 °C in H_2 (relative to the particles formed following treatment at 200 °C in H_2).

(36) The stated bond distance for this contribution may be spuriously short as a consequence of multiple scattering effects that were not taken into account by the reference file used. Because the assignment of this

nonbonding shell, which is located far from the absorber (Rh) atom in comparison with the shells (Rh−Rh and Rh-support) of interest, is tentative and its exact geometry relative to the absorber atom not well-defined, no attempt was made to correct for the influence of multiple scattering.

(37) (a) Chini, P.; Martinengo, S. *Inorg. Chim. Acta* **1969**, *3*, 21. (b) Chini, P.; Martinengo, S. *Inorg. Chim. Acta* **1969**, *3*, 299. (c) Chini, P.; Martinengo, S. *Inorg. Chim. Acta* **1969**, *3*, 315.

(38) Evans, J.; McNulty G. S. *J. Chem. Soc., Dalton. Trans.* **1984**, 587.

(39) Rao, L.-F.; Fukuoka, A.; Kosugi, N.; Kuroda, H.; Ichikawa, M. *J. Phys. Chem.* **1990**, *94*, 5317.

(40) Mantovani, E.; Palladino, N.; Zanobi, A. *J. Mol. Catal.* **1977/8**, *3*, 285.

(41) Davis, M. E.; Rode, E. J.; Taylor, D.; Hanson, B. E. *J. Catal.* **1984**, *86*, 67.

(42) Rode, E. J.; Davis, M. E.; Hanson, B. E. *J. Catal.* **1985**, *96*, 574.

(43) Smith, A. K.; Hugues, F.; Theolier, A.; Basset, J.-M.; Ugo, R.; Zanderighi, G. M.; Bilhou, J. L.; Bilhou-Bougnol, V.; Graydon, W. F. *Inorg. Chem.* **1979**, *18*, 3104.

(44) Solution chemistry indicates that chloride ions lower the rate at which rhodium cations are reduced and influence which rhodium carbonyl is produced.

(45) The TiO_2 (Degussa P25) was formed by hydrolysis of $TiCl_4$, which results in trace chlorides in the oxide. However, the manufacturer reported Cl concentrations to be less than a few ppm.

(46) Goellner, J. F.; Guzman, J.; Gates, B. C., to be published.

(47) Zhao, A.; Gates, B. C. *Langmuir* **1997**, *13*, 4024.

(48) Triantafillou, N. D.; Gates, B. C. *Langmuir* **1999**, *15*, 2595.

(49) Smith, A. K.; Theolier, A.; Basset, J.-M.; Ugo, R.; Commereuc, D.; Chauvin, Y. *J. Am. Chem. Soc.* **1978**, *100*, 2590.

(50) Yates, J. T.; Basu, P.; Panayotov, D. *J. Am. Chem. Soc.* **1988**, *110*, 2074.

(51) After treatment at 400 °C, the Rh−C contribution was no longer detected. The carbon-containing residue had likely desorbed, and the Rh_6 octahedra were no longer stabilized on the surface of $TiO_{2,200}$. We speculate that at temperatures greater than 200 °C these carbon-containing species (possibly having been hydrogenated to give less strongly bound adsorbates) probably desorbed, leaving the Rh_6 octahedra less resistant to sintering in the H_2 atmosphere (and the water formed in it).

(52) Ferrari, A. M.; Neyman, K. M.; Mayer, M.; Staufer, M.; Gates, B. C.; Rösch, N. *J. Phys. Chem. B* **1999**, *103*, 5311.

(53) Goellner, J. F.; Neyman, K. N.; Mayer, M.; Nörtemann, F.; Gates, B. C.; Rösch, N. *Langmuir*, **2000**, *16*, 2736.

(54) Yang, A. C.; Garland, C. W. *J. Phys. Chem.* **1957**, *61*, 1504.

(55) (a) Smith, G. C.; Chojnacki, T. P.; Dasgupta, S. R.; Iwatate, K.; Watters, K. L. *Inorg. Chem.* **1975**, *14*, 1419. (b) Chini, P. *J. Chem. Soc., Chem. Commun.* **1967**, *67*, 441.